On the Inversion of Limb Radiance Measurements I: Temperature and Thickness[1]

JOHN C. GILLE[2]
Dept. of Meteorology and Geophysical Fluid Dynamics Institute, Florida State University, Tallahassee
AND FREDERICK B. HOUSE[3]
Physics Dept., Drexel University, Philadelphia, Pa.

(Manuscript received 2 June 1971)

ABSTRACT

The calculation of limb radiance as a function of tangent height is shown to require the vertical distribution of temperature and the pressure at one level. Conversely, given the limb radiance curve and the pressure corresponding to one tangent point, it is possible to determine the temperature profile as a function of height relative to the given level, using an iterative technique. If the given pressure is incorrect, there will be systematic errors in the inferred temperatures. This feature may be used to determine the correct pressure by requiring that temperatures inferred from measurements in two spectral regions of differing opacities agree. Results of inverting synthesized realistic data are presented. The data include the effects of water vapor and ozone contamination of the carbon dioxide signal, instrument field of view, and random and systematic noise for real atmospheres having small-scale vertical structure. Results indicate that the temperature may be obtained from the tropopause to 60 km with an rms error <3K. The thickness between the 10- and 1-mb surfaces may also be determined to ± 50 m. For measurements spaced 1000 km apart in mid-latitudes, this will yield thermal winds to ± 7 m sec^{-1}. Contemplated improvements in the alogrithm and the likelihood of achieving smaller noise figures than those used in the study indicate that better temperature and thickness accuracies and inferences to higher altitudes should be attainable with a real instrument.

1. Introduction

Since the early days of the space program, infrared horizon sensors have been used to obtain attitude information for earth-orbiting satellites. Several early studies (Hanel *et al.*, 1963; Kondrat'yev and Yakushevaskaya, 1963; Wark *et al.*, 1964) computed the outgoing thermal radiance at the earth's limb from assumed temperature, moisture and ozone profiles in several spectral intervals. Subsequent studies (Bates *et al.*, 1967; Bates, 1967; Gille, 1968) have employed more sophisticated calculational schemes. Early satellite (Bandeen *et al.*, 1963) and rocket (Walker *et al.*, 1966) measurements could only show qualitative agreement, but later rocket measurements (McKee *et al.*, 1968; Whitman *et al.*, 1968; Girard and Lemaitre, 1970) have shown quantitative agreement with the calculations.

This opens the possibility of inverting measurements of outgoing radiation to obtain information about the atmosphere. The geometry of limb viewing is shown in Fig. 1. A satellite-borne radiometer receives the radiation emitted by the atmosphere along a ray path that may be identified by the height (tangent height) or the point (tangent point) closest to the surface. The atmosphere may be scanned by sweeping the view direction from tangent heights <0 (ray paths intersecting the surface) to large positive values. The following advantageous features of limb scanning are apparent from a consideration of Fig. 1.

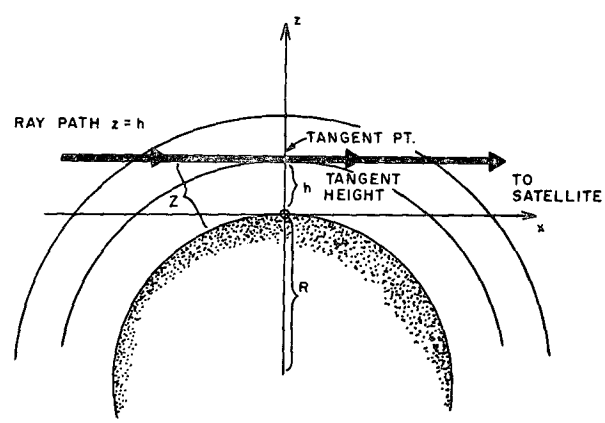

FIG. 1. The geometry of limb viewing.

[1] Geophysical Fluid Dynamics Institute Contribution No. 46.
[2] Part of this research was performed while visiting the University of Colorado and the National Center for Atmospheric Research, Boulder, Colo. The National Center for Atmospheric Research is sponsored by the National Science Foundation.
[3] Part of this research was performed while at GCA Corporation, Bedford, Mass.

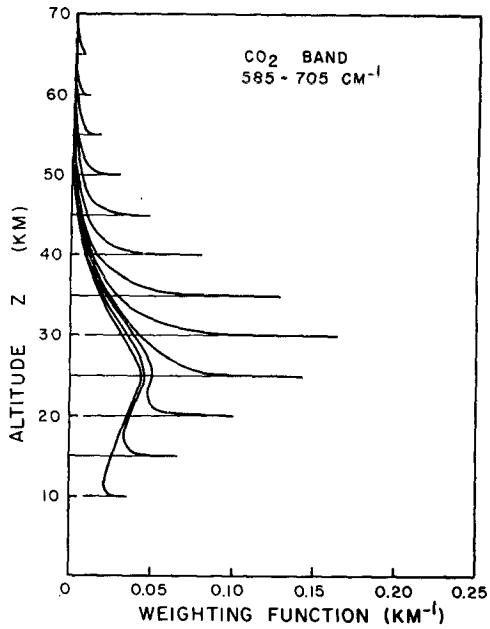

FIG. 2. Limb viewing weighting function $W(h; z)$ [defined in Eq. (1)] for the ideal case of an instrument with an infinitesimal vertical field of view. These are computed for the spectral band 585–705 cm^{-1}, covering most of the 15-μm band of CO_2.

1) *High inherent vertical resolution.* For geometric reasons, none of the signal originates below the tangent point. If the atmosphere is divided up into shells of uniform thickness above the tangent point, the shell immediately above the tangent point will contain the longest horizontal segment of the ray path. Because atmospheric density and pressure fall off exponentially with height, a large fraction of the outgoing radiation originates in the few kilometers immediately above the tangent point, if the whole atmosphere along the path is moderately transparent. Mathematically, the outgoing radiance I received when viewing tangent height h may be written as

$$I_i(h) = \int_0^\infty B_i(z) W_i(h; z) dz, \qquad (1)$$

where the subscript i denotes the spectral interval, B the Planck blackbody function, z the vertical coordinate, and $W(h; z)$ the weighting function, indicating how much height z contributes to the radiance along the ray path through h.

Fig. 2 shows weighting functions for a wide spectral interval (585–705 cm^{-1}), covering most of the absorption by the 15-μm band of carbon dioxide, for an instrument with an infinitesimal vertical field of view. For tangent heights above $\sim$25 km, the major part of the contribution comes from within $\sim$3 km of the tangent height. Below 25 km, the weighting functions begin to take on the broad shape of the nadir-viewing weighting functions (e.g., Wark, 1970; Smith, 1970), although there is still a spike at the tangent point, due to the less strongly absorbing wings of the band. These provide information about deeper regions of the atmosphere.

These narrow weighting functions give an indication of the theoretically attainable vertical resolution. A real instrument has a finite field of view, and its weighting functions, resulting from convolutions of ones like those in Fig. 2, would be broader.

2) *Black (and constant) background.* For $h>0$, all radiation received originates in the atmosphere, and all variations in signal are due to atmospheric variations. The ambiguity that occurs when nadir-viewing instruments can see a changing underlying surface is absent.

3) *Large opacity.* There is 60 times more emitting material along a horizontal path grazing the surface then there is in a vertical path to that tangent point, and the factor gets larger as the tangent height is increased. This means that for a broad spectral band a measurable signal will be received from considerably higher altitudes than will be sounded by "broad band" vertical viewing, although the latter can be improved by selective chopping of the signal (Houghton and Smith, 1970).

4) *Large surface coverage.* The view direction from the satellite can be oriented in any azimuthal direction relative to the satellite motion, and can be stepped from azimuth to azimuth. A satellite in earth orbit at 1000 km altitude would see over 3300 km to the left and right of the orbit, while at 1500 km the figure is 3950 km.

There are, of course, disadvantages associated with these features. The long paths mean that, even for rather transparent spectral regions, we will have difficulty seeing the solid surface of the planet. A cloud along a path will act as a body of infinite opacity, and may cause a considerable alteration in the emerging radiation. For the earth's atmosphere, where clouds are present but usually below the tropopause, these facts suggest that reliable operation will be limited to the upper troposphere and above, with even the coverage of the upper troposphere and lower stratosphere being subject to occasional interruption. For these reasons we present solutions only above a nominal tropopause at 15 km.

The sharp vertical weighting function is associated with a horizontal region that may stretch 200 km or more along the ray path (see, e.g., Bates, 1967, Fig. 15). This could lead to problems of interpretation if large changes in the atmospheric state occurred over this distance. However, all evidence suggests that the length scales for stratospheric and mesospheric temperature changes are very large except for limited polar regions during sudden warming situations. In such cases, allowances may be made. In this paper, all atmospheres are assumed to be spherically symmetrical.

Previous studies (Bates *et al.*, 1967; Gille, 1968) have shown that refractive effects are small in the stratosphere and above. Accordingly, although one would want to include them when inverting real observations, they have not been included in this study. Their omission will not alter the conclusions reached.

Examples of calculated profiles of limb radiance as functions of tangent height are shown for a mid-latitude winter sounding (see Section 5) in Fig. 3. The wide (W) channel refers to the 585–705 cm^{-1} channel discussed above. The narrow (N) channel covers 630–685 cm^{-1}, the intensely absorbing center of the 15-μm bands of CO_2. The signals are quite similar at upper levels, where only the strong lines near the centers of the bands are contributing. Below about 30 km, the W signal is much larger because the weaker lines in the band wings are contributing energy from the lower atmosphere. The dashed line presents the difference between W and N signals, or the contribution from the 585–630 cm^{-1} and 685–705 cm^{-1} regions. The steeply sloping portions of the curve occur in situations where the whole path through the atmosphere is moderately transparent, and an appreciable portion of the signal is coming from the tangent point. Fig. 3 demonstrates that the W−N region provides better information on the lower levels of the stratosphere and upper levels of the troposphere. It is also of interest to compare the signal to the 0.01 W m^{-2} sr^{-1} random noise used in the simulations described in Section 5.

Gille (1968) pointed out that useful information about the stratopause region could be obtained from precise satellite measurements without inverting the data. Several investigators (McKee *et al.*, 1969; House and Ohring, 1969; Burn and Uplinger, 1970) have explored the inversion of such data, applying their techniques to the rocket measurements mentioned above. In all these cases, the assumption was made that the radiance must be measured as a function of tangent height, presupposing knowledge of the absolute directions of the lines of sight. Because of the sharp fall-off of radiance with tangent height (Fig. 3), Gille (1968) noted that the attitude requirements are very stringent. They can be met, but expensive instrumentation and data processing are required.

In this paper we show how the unique temperature solution may be obtained as a function of pressure or, alternatively, as a function of relative attitude, from radiance measurements in two channels with different spectral characteristics, and knowledge of the *relative* pointing direction only. Simply stated, by demanding that the solution obey the hydrostatic equation as well as produce the measured radiance profiles in the two channels, a unique temperature distribution is determined.

In Section 2 the inversion problem is formulated. Sections 3 and 4 cover the methods of temperature inversion and determination of a parametric pressure p_0, respectively. Some results of inversions of realistic data are shown and summarized in Section 5. Our conclusions are stated in Section 6.

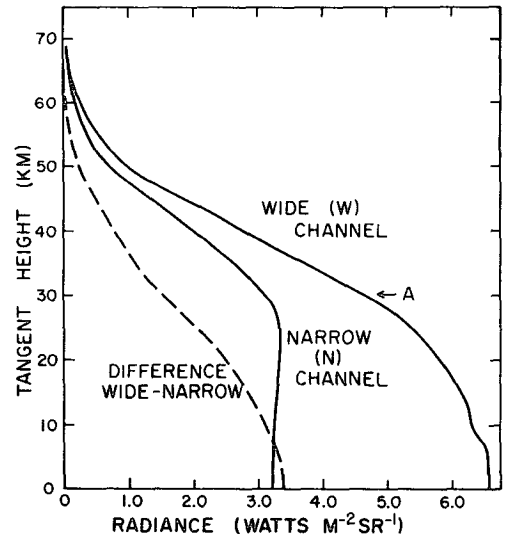

FIG. 3. Limb radiance as a function of tangent height for wide (585–705 cm^{-1}) and narrow (630–685 cm^{-1}) channels in the 15-μm band of CO_2. Their difference results from emission by generally weaker lines away from the band center, and provides information on deeper atmospheric layers. Point A is discussed in Section 2.

2. Formulation of the limb radiance inversion problem

From the geometry of Fig. 1, and noting that the background is cold space, the radiative transfer equation for a non-scattering atmosphere in local thermodynamic equilibrium may be written as

$$I_i(h) = \int_{-\infty}^{\infty} B_i[T] \frac{d\tau_i(h; x)}{dx} dx, \qquad (2)$$

where, in addition to the symbols defined above, T is temperature, x the distance coordinate along the ray path, with the origin at the tangent point and positive toward the satellite (located at $+\infty$), and $\tau(h; z)$ the mean transmission in the spectral interval along the path with tangent height h from point x to the satellite. In subsequent discussions the subscript i will be understood, and suppressed.

The temperature inversion problem is to determine B and therefore T from measurements of I, assuming that $d\tau/dx$ is known. The latter requires that the distribution of the emitting species be known, which in practice means that radiation from CO_2, a uniformly mixed gas, is measured. In the limb problem $d\tau/dx$ is also crucially affected by the atmospheric structure, as will appear presently.

Ideally, $\tau(h; x)$ should be obtained from measurements under atmospheric conditions, or from a point-by-point integration across the spectrum. Because of the broad bands that one may use in limb scanning, we anticipate that band models will be reasonably accurate, and certainly sufficient for the following heuristic argument. In general, τ will depend on the absorber amount along the path between the point x and the satellite, given by

$$a(h; x) = c \int_x^\infty \rho(x')dx', \tag{3}$$

and the pressure and temperature distribution along the path. In (3), c is the mixing ratio, assumed constant, and ρ the atmospheric density. We may write (Goody, 1964)

$$\tau(h; x) = \tau(h; \bar{a}, \bar{p}),$$

in which $\bar{a}$ and $\bar{p}$ are temperature weighted absorber amount and a temperature and mass weighted mean pressure. Following Rodgers and Walshaw (1966), we define

$$\left.\begin{aligned} \bar{a} &= c \int_x^\infty \Phi[T(x')]\rho(x')dx' \\ \bar{a}\bar{p} &= c \int_x^\infty \psi[T(x')]p(x')\rho(x')dx' \end{aligned}\right\}. \tag{5}$$

Incorporating (4) and (5) in (2), and converting to a vertical integral results in

$$I(h) = \int_h^\infty B[T(z)]c\rho(z)\left|\frac{dx}{dz}\right|_z \left\{\Phi(z)\left[-\left[\frac{\partial\tau(h; \bar{a}, \bar{p})}{\partial\bar{a}}\right]_a - \left[\frac{\partial\tau(h; \bar{a}, \bar{p})}{\partial\bar{a}}\right]_p\right] - \frac{\psi(z)p(z) - \Phi(z)\bar{p}(z)}{\bar{a}(z)} \times \left[\left[\frac{\partial\tau(h; \bar{a}, \bar{p})}{\partial\bar{p}}\right]_a - \left[\frac{\partial\tau(h; \bar{a}, \bar{p})}{\partial\bar{p}}\right]_p\right]\right\} dz, \tag{6}$$

where subscripts a and p refer to positions on the path at elevation z *anterior* and *posterior* to the tangent point, since x is a double-valued function of z, and dx/dz is a geometric factor associated with going from a horizontal to a vertical integral. For convenience let us denote the expression in braces as $L(h; z)$. We note in passing that

$$W(h; z) = c\rho(z)\left|\frac{dx}{dz}\right|_z L(h; z).$$

Assuming the atmosphere is in hydrostatic balance and obeys the ideal gas law with specific gas constant R, the density at z is

$$\rho(z) = p_0[RT(z)]^{-1} \exp\left[-\int_{z_0}^z \frac{gdz'}{RT(z')}\right], \tag{7}$$

where $p = p_0$ at $z = z_0$. Inserting (7) in (6) immediately yields

$$I(h - z_0) = p_0 cR^{-1} \int_{h-z_0}^\infty B[T(z)]\left|\frac{dx}{dz}\right|_z L(h; z) \times \exp\left[-\int_{z_0}^z gR^{-1}T(z')^{-1}dz'\right] T(z)^{-1}dz. \tag{8}$$

In writing (8), we have made use of the fact that z_0 is the only fixed altitude that appears, and other altitudes may be measured relative to it. Given a radiance profile, like one of those in Fig. 3 but with no attached tangent height scale, we may pick a particular point on the curve (such as A in Fig. 3) and designate its height as z_0. Other tangent heights are then measured relative to z_0, which appears only as a reference level whose absolute value is not required. In the inversion problem, we have measurements of $I(h - z_0)$ and wish to determine $T(z - z_0)$. Clearly, p_0 will be a crucial quantity in the procedure. The inversion problem may then be separated into two parts, i.e.,

1) Given p_0 and measurements of $I(h - z_0)$, can $T(z - z_0)$ be obtained?
2) How may p_0 be determined?

These questions are discussed in Sections 3 and 4, respectively.

3. Temperature profile determination when p_0 is known

We now consider the situation in which the radiance is measured as a function of distance from the elevation z_0, which is not known but at which the pressure is known to be p_0. The complex nature of the temperature dependence on the right-hand side of (8) suggests an iterative scheme. The narrow weighting functions indicate that Chahine's (1968, 1970) technique of using one measurement to correct the value at one level should be particularly applicable, and in fact the radiance measured at tangent height $h - z_0$ may be used to correct the temperature at that altitude. For convenience, let us write the altitude relative to z_0 as $h_j^* = h_j - z_0$. The subscript j denotes a particular tangent height, since ordinarily the radiance is sampled rather than measured continuously. The steps in the solution are as follows:

1) An initial temperature profile $T^0(h^*)$ is assumed. (The superscript indicates the order of iteration.)
2) The temperature profile, $T^n(h^*)$ in the nth iteration, is used with p_0 and the hydrostatic equation to distribute the atmospheric mass in altitude. This is important because it controls the amount of material $a(h^*; x)$ in a particular path.
3) The outgoing radiance $I^n(h_j^*)$ is calculated from one of the equivalent equations (2), (6) or (8). [Usually (2) is used.]

4) The calculated outgoing radiance $I^n(h_j^*)$ is compared to the observed value, $I_0(h_j^*)$. If a convergence criterion is satisfied, the temperature profile is accepted as the solution. A typical convergence criterion is that the rms difference between the calculated and measured radiances, over the profile, be reduced to somewhat less than the noise of the radiometric measurements.
5) If the convergence criterion is not met, the differences between the calculated and observed radiances are used to adjust the temperature profiles according to a relaxation equation.

A straightforward relaxation expression may be derived from the "instant inversion" scheme suggested by J. I. F. King and used by House and Ohring (1969). The delta-function spike of the weighting function suggests that one may write (8) as

$$I(h_j^*)=B(h_j^*)\epsilon(h_j^*), \tag{9}$$

where $\epsilon(h_j^*)$ is the effective emissivity of the atmospheric path. Physically, (9) is equivalent to putting all the opacity close to the tangent point, or having all the outwelling radiation originate there. Neglecting the temperature dependence of $\epsilon(h_j^*)$, logarithmic differentiation results in

$$\frac{dI(h_j^*)}{I(h_j^*)}=\frac{1}{B(h_j^*)}\frac{\partial B(h_j^*)}{\partial T}dT=\frac{c_2\bar{\nu}}{T(h_j^*)^2}dT(h_j^*), \tag{10}$$

in which c_2 is the second radiation constant, $\bar{\nu}$ the mean frequency, and we have noted that the energy of the radiative transition is much greater than the thermal energy of the molecules. The relaxation equation is then

$$T^{n+1}(h_j^*)=T^n(h_j^*)+\frac{2T^n(h_j^*)^2}{c_2\bar{\nu}}\left[\frac{I_0(h_j^*)-I^n(h_j^*)}{I_0(h_j^*)+I^n(h_j^*)}\right]. \tag{11}$$

Eq. (11) permits the $(n+1)$st temperature profile to be computed from the differences between the measured radiances and the calculations from the nth iteration. The new profile is used in step 2, and the process repeated until the convergence criterion is met. In the case when the results are inferred every 2 or 3 km, intermediate temperatures are linearly interpolated and used to calculate the I^n's.

This technique has been applied to the inversion of ideal radiances (no noise, infinitesimal vertical field of view) calculated for a real mid-latitude winter sounding in the 585–705 cm^{-1} channel. The initial guess was the standard atmosphere, inverted levels were 1 km apart, and the iteration was continued until the rms difference between the observed and calculated radiance was less than 0.01 W m^{-2} sr^{-1} (which was taken as a rough indication of the noise to be expected in a real instrument). The results are shown in Fig. 4, in which the solid line is the actual profile and the dots indicate the inversion solution. (The dashed line is discussed later.) Starting with an initial guess of an isothermal atmosphere at 200 or 300K did not change the temperature at any level by more than a few hundredths of a degree. The overall shape of the curve, as well as many smaller features are followed with astonishing fidelity. In particular, the thin, sharp feature at 37 km is reproduced quite well. The rms temperature error between the initial sounding and the inversion from 15–60 km was 0.9K, achieved after eight iterations. Continuing iteration leads to continuing reduction in the rms differences in the radiances, and improvement in the temperature. Thus, if p_0 is known, the temperature structure may be inferred. McKee (1970) has also obtained temperature solutions as functions of pressure without absolute attitude information, starting from the top of the sounding (about 60 km) and working down in a layer-by-layer manner.

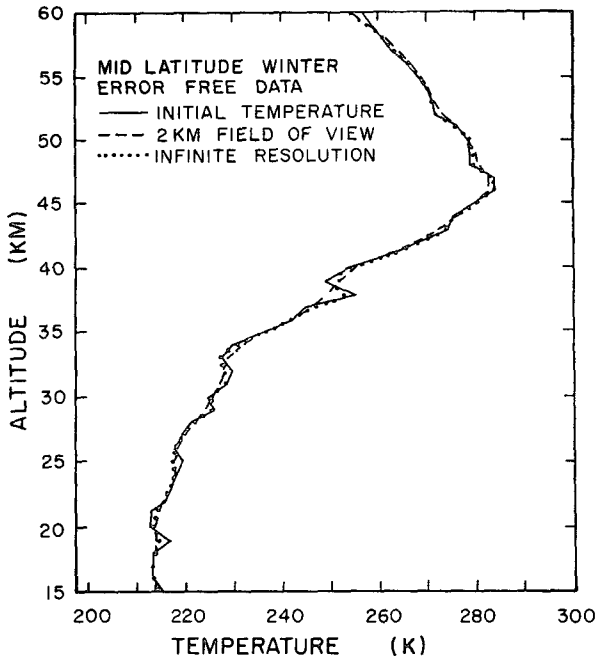

FIG. 4. Solution obtained by inverting noise-free data with infinite vertical resolution (dotted line) compared to the actual mid-latitude winter sounding (solid line). Inversion of noise-free data with a 2-km field of view (dashed line) is discussed in Section 5d.

In this formulation, the solution is obtained as a function of height relative to z_0. With p_0 and the accurately known relative heights, the hydrostatic equation can be integrated to yield the temperature as a function of pressure, as the conventional radiosonde does.

To get the altitude of the temperature profile above the surface, it is only necessary to have the altitude of one pressure level from about 120 to 0.4 mb from any data source. This other source could be the analyzed maps based on radiosonde soundings, satellite data (e.g., IRIS or SIRS), or a balloon with a radio altimeter,

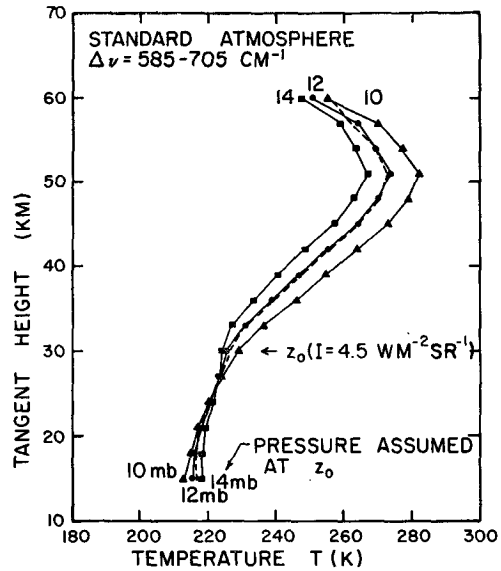

FIG. 5. Dependence of inferred solutions on p_g. The dashed line is the true profile, the U. S. Standard Atmosphere. Solid lines are inversion solutions with the values 10, 12 and 14 mb assumed for p_g. Correct value is 12 mb.

such as one being considered for GARP. Alternatively, climatological data could be used. For instance, Smith (1969a) indicates that the standard deviation of the height of the 50-mb surface is only 0.1 km. Thus, it seems feasible to locate a given temperature profile or feature rather precisely in altitude.

4. Determination of p_0

a. Dependence of solutions on p_0

From Eq. (8), it is clear that p_0 occupies a critical position in the inversion. In general, however, when we designate z_0 we will not know p_0 and a value p_g must be guessed. The dependence of the inverted solutions on p_g is shown in Fig. 5. In this illustrative example, radiances have been calculated for the U. S. Standard Atmosphere (dashed line), and inverted with three different assumed values of p_g at a level where the radiance was 4.5 W m^{-2} sr^{-1}. (The initial guess was an isothermal atmosphere at 250K). The inverted values (points) are spaced 3 km apart.

We see that if the guessed pressure p_g exceeds p_0, temperature determinations at upper levels are systematically too small, while those at lower levels are too large. The reverse occurs for $p_g<p_0$. Between upper and lower levels is a level which is nearly invariant with p_g.

These results are understandable with the following heuristic argument. Let us make the approximations that the transmission is a simple exponential

$$\tau = e^{-ka(h^*;x)},$$

and, because of the sharp weighting functions, that all the radiation is coming from the region of the tangent point. Then (6) becomes

$$I(h_j^*) \approx 2B(h_j^*)c\left|\frac{dx}{dz}\right|_{h_j^*} k \exp[-ka(h_j^*,0)]\rho(h_j^*)\Delta z. \quad (12)$$

Solving for B, we have

$$B(h_j^*) = \frac{I(h_j^*)}{2ck\rho(h_j^*)\exp[-ka(h_j^*,0)]\left|\frac{dx}{dz}\right|_{h_j^*}\Delta z}. \quad (13)$$

For a level where $ka<1$, if our densities are larger than the true value, the increased ρ will overcome the decrease in e^{-ka}, leading to small values of B and T. Where $ka>1$, the decrease in e^{-ka} dominates the increased ρ, leading to large B and T. The opposite occurs for densities less than the true value.

This is made explicit if we note that an error in p_g multiplies the correct densities by $p_g/p_0=1+\delta$. A simple expansion about the correct values shows that

$$B(h_j^*) = \frac{I(h_j^*)}{2ck\rho_0(h_j^*)\left|\frac{dx}{dz}\right|_{h_j^*}\exp[-ka_0(h_j^*,0)]\{1+\delta[1-ka_0(h_j^*,0)]\}}, \quad (14)$$

where subscript zero indicates the correct value.

The effect of p_0 errors is now clear. For p_g too large ($\delta>0$), for upper levels at which $ka_0(h_j^*,0)<1$, the denominator will be too large, and consequently B (and T) will be too small. Conversely, at lower levels where $ka_0(h^*,0)>1$, the denominator is too small, and B too large. When $ka_0(h^*,0)=1$, the result is correct, regardless of δ. The opposite occurs for $\delta<0$. Eq. (14) clearly reproduces the features observed in Fig. 5 and, in particular, the correct temperature that is obtained when $ka_0(h^*,0)$, the optical depth to the tangent point, is equal to unity.

Note that there is no way to choose between solutions on meteorological or mathematical grounds. There is a range of values of p_g which yield meteorologically acceptable solutions. The residuals decrease as rapidly and as far for the incorrect as for the correct solutions. The reason is obvious from (8), where we are using N measurements of I to determine T at N heights. At least one additional datum is needed to define p_0.

Possibly $N-n$ measurements could be used to determine T, and n values to determine p_0. The latter would require that we make some assumption about the

solution, which is not very appealing and, in view of the anomalous soundings that can occur, would probably not be very satisfactory.

Alternatively, the temperature at a given pressure in the range of the solutions (except near $ka_0=1$) will uniquely determine the correct solution. This information could come from an analysis of conventional temperature data at 100, 50 or 30 mb, or from data from constant density balloons with temperature sensors. Both possibilities have weaknesses because of the likelihood that coverage of the Southern Hemisphere and oceanic regions would be very sparse.

It is possible that data from a nadir-viewing temperature sounder (e.g., SIRS, IRIS) could be used. There are immediate complications because a limb viewer is looking at a different geographical region from a nadir sounder on the same spacecraft. Additionally, the largest errors of nadir retrievals at present are located near the tropopause (Smith, 1970; Wark, 1970) where one would like best accuracy because it is in this region that the limb solutions are most sensitive to p_g. Although interesting, this does not now appear to be the most promising approach.

b. Measurements in two spectral channels

The invariance of the correct temperature at the level where $ka_0(h^*,0)=1$ immediately suggests that a second spectral channel (designated by subscript 2), with $k_2a_0(h^*,0)=1$ at a different level, will lead to a second correct temperature point, and uniquely select the correct p_0 and solution from the family of those satisfying the first channel measurements. This is indicated schematically in Fig. 6. Some solutions for the more opaque (O) channel are indicated by dashed lines, and for the more transparent (T) channel by dotted lines. The correct solution is the solid line passing through both the invariant points.

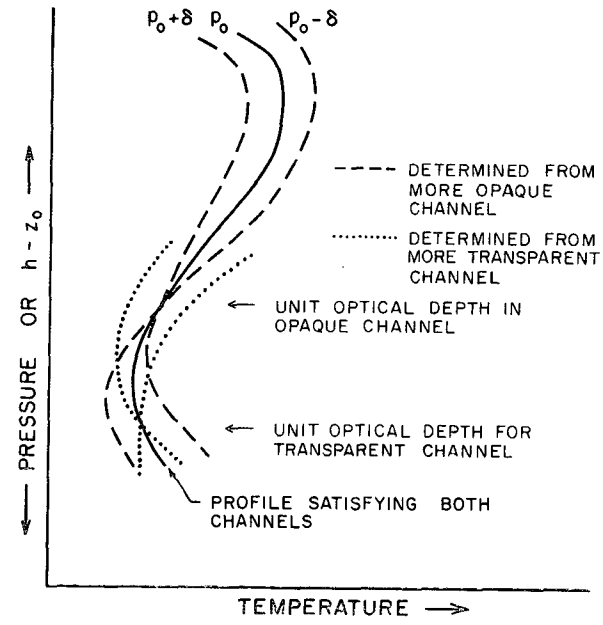

FIG. 6. Schematic diagram of the two-channel method for obtaining a unique solution.

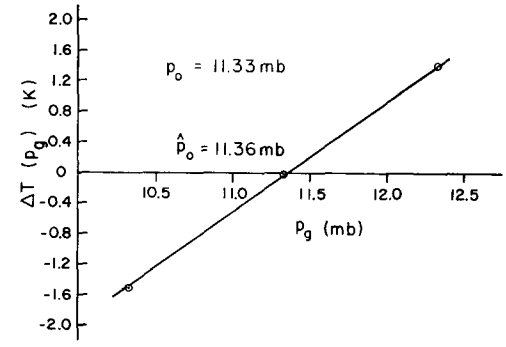

FIG. 7. Mean temperature difference $\Delta T(p_g)$ between the W and N channel inversions over the 21–30 km height range as a function of p_g. $\Delta T=0$ for $\hat{p}_0=11.36$ mb, close to $p_0=11.33$ mb.

Fig. 6 also indicates that the two temperature determinations do not agree unless p_0 is correct. When $p_g>(<)p_0$, the temperature determined from the O channel is greater (less) than that determined from the T channel.

We can put this on a more quantitative basis with our simplified model. If we make measurements in two spectral channels, and require that the two inversions yield the same temperature at the same level, we have from (14)

$$\frac{I_1(h_j^*)}{k_1\exp[-k_1a_g(h_j^*,0)]\{1+\delta[1-k_1a_g(h_j^*,0)]\}} = \frac{RI_2(h_j^*)}{k_2\exp[-k_2ag(h_j^*,0)]\{1+\delta[1-k_2a_g(h_j^*,0)]\}}, \quad (15)$$

in which subscript g denotes values based on p_g, and $R=B_1(T)/B_2(T)$ is a slowly varying function of temperature. All quantities in (15) are known except δ. Upon solving for δ, the determined value of p_0 may be obtained from

$$p_0=p_g(1+\delta).$$

In the realistic case of imperfect measurements, we will not make optimum use of our data by using only one level to determine δ. Because the solutions in the two channels depend on p_g, we may write them as $T_{1,2}(h_j^*;p_g)$. Comparing the solutions over a region in which they have comparable accuracy, a quantity which indicates the size of the error and the direction in which p_g must be changed is

$$\Delta T(p_g)=\frac{1}{N_2-N_1+1}\sum_{j=N_1}^{N_2}T_1(h_j^*;p_g)-T_2(h_j^*;p_g). \quad (16)$$

Fig. 7 displays $\Delta T(p_g)$, the difference between temperatures inferred in the W and N channels de-

TABLE 1. Temperature profiles and situations.

Temperature profile (atmosphere number)	Geographic region	Season	Location of sounding	Latitude (N)	Date
1	Mid latitude (Key profile)	Winter	Wallops Island	38	31 Jan. 1967
2	High latitude	Winter	Fort Greely	64	20 Jan. 1967
3	High latitude	Winter (stratwarm)	Fort Greely	64	20 Mar. 1967
4	High latitude	Summer	Fort Churchill	59	28 May 1965
5	Low latitude	Spring	Antigua	17	13 Apr. 1966
6	Mid latitude	Spring	Wallops Island	38	27 May 1965

scribed above, averaged over the 21–30 km region of tangent height, vs p_g for the mid-latitude winter sounding discussed previously. In this range the dependence is linear, and the zero crossing occurs at a pressure close to p_0. This suggests that a good operational algorithm for obtaining an estimate $\hat{p}_0$ of p_0 is

$$\Delta T(\hat{p}_0)=0. \tag{17}$$

Eq. (17) was used in the results described below.

Alternatively, one can define the root mean square (rms) temperature difference between the two determinations, and test the algorithm

$$\Delta T_{\text{rms}}(p_0)=\min \Delta T_{\text{rms}}(p_g).$$

Numerical results showed that the curve of $\Delta T_{\text{rms}}(p_g)$ vs p_g had a broad minimum, leading to an undesirable $\hat{p}_0$ sensitivity to small errors. Because more computations were required to define the curve, this approach was abandoned in favor of the one leading to (17).

5. Results of inverting realistic data

a. Introduction

Any inversion method should yield very good results for synthesized data that are noise-free and perhaps ideal in other ways as well. In practical applications, an inversion routine must return useful results in the presence of noise and other instrumental limitations. For limb scanning, the vertical field of view is an important instrumental parameter because of the rapid variation of radiance with tangent height. Observations of the type necessary to test the inversion method discussed above are apparently not available at the present time. To allow an accurate assessment of its capabilities, realistic data have been synthesized and inverted for a variety of conditions.

b. Synthesis of realistic data

1) SELECTION OF SAMPLE ATMOSPHERES

To obtain adequate geographical and seasonal coverage, while limiting the amount of computation necessary, several representative temperature, ozone and water vapor distributions were chosen. The latter were necessary because these gases make a small contribution to the signal in the spectral bands chosen.

2) TEMPERATURE PROFILES

A desideratum was that the atmospheres have considerable fine-scale structure. This was partly because the sharpness of the CO_2 weighting functions suggested that small features could be successfully retrieved, and partly because of a desire to determine how well the p_0 determination scheme would work in the most difficult cases.

The profiles were selected visually, and, as atmospheres with very fine-scale structure appear more jagged than those with broader variations, there was a tendency to emphasize the former at the expense of the latter.

The situations and profiles selected are listed in Table 1. Because there are more variations and more interesting phenomena at high latitudes (e.g., the stratospheric warmings), more examples of these are included. Low latitude variation is small, and the sounding used is representative of the whole year, although a colder tropopause is generally the case in the tropics.

3) OZONE PROFILES

The data sources for the ozone distributions are summarized in Table 2. There are few observations above balloon altitudes. The rocket observations used in Profiles 1 and 2 are among the most recent, and apparently the best. They represent high-latitude winter and mid-latitude autumn conditions. In addition to observed values, it was felt desirable to use distributions based on photochemical theory. Profile 3, based on an oxygen-only reaction scheme with modern reaction coefficients, is probably a considerable overestimate. Profile 4 is believed to be more realistic.

4) WATER VAPOR PROFILES

The data sources used for the water vapor profiles are listed in Table 3. Profiles 1 and 2 are based largely on the measurements of Mastenbrook (1968). Profile 3 is considered a lower bound; the values are consistent with some spectrometric measurements. Profile 4 is based on the measurements of Sissenwine *et al.* (1968), on the U. S. West Coast. Whether a real or instrumental difference exists between his results and Mastenbrook's

is not known. Profiles 1 and 2, although they differ only slightly, are representative of high latitude summer and low latitude conditions.

5) COMPOSITE ATMOSPHERIC PROFILES

Composite atmospheres, having distributions of temperature, ozone and water vapor, were selected and designated by the three numbers of the component profiles. The first of each profile was designated as the "key" profile, on which many exploratory calculations were run. The composite key profile is then designated as 111.

To study the effect of ozone variations on temperature determination, the set 111, 121, 141 was selected. To assess the effect of water vapor, 144 was added.

Additional geographic situations were chosen, with reasonable or upper bound amounts of constituents, 211, 313 (allowing for much more ozone during the time of a stratowarm), 522 to give a tropical situation, and 644 for a mid-latitude reasonably ozone-rich and moist condition.

The eight composite atmospheres were then 111, 121, 141, 144, 211, 213, 522, 644.

6) TRANSMISSION DATA

Smith's (1969b) transmission data were used in 5-cm^{-1} intervals for water vapor and carbon dioxide. For the 14-μm band of O_3, Goody's random band parameters and temperature correction coefficients were calculated by Gille (in preparation) from unpublished line parameters computed by Clough. Temperature and pressure variations along the path were treated by the extended Curtis-Godson approximation described in Rodgers and Walshaw (1966).

7) CHANNEL SELECTION

The two-channel inversion scheme to obtain p_0 information requires that one channel be more transparent than the other. The criterion that guides the choice of the opaque channel is that it be in the center of the band, and broad enough to receive enough energy to ensure an adequate signal-to-noise ratio. In addition,

TABLE 2. Sources of ozone profile data.

Temperature profile (atmosphere number)	Surface to 20 km	Above 20 km
1*	Komhyr and Sticksel (1967) Ozonesonde, Fairbanks, 2 March 1965	Hilsenrath (1971) Rocket observation
2	Komhyr and Sticksel (1967) Ozonesonde, Sterling, Va.,	Hilsenrath *et al.* (1969) Rocket observation
3	Komhyr and Sticksel (1967) Ozonesonde, Sterling, Va., 25 March 1963	Hunt (1966a) Classical O_3 theory
4	Komhyr and Sticksel (1967) Ozonesonde, Canton Island, 4 November 1965**	Hunt (1966b) Modified O_3 theory

* Key profile.
** Sounding to 26 km, theory above.

TABLE 3. Sources of water vapor profile data.

Temperature profile (atmosphere number)	Lower stratosphere	Upper stratosphere
1*	Mastenbrook (1968) Balloon sounding, Thule, Greenland	Scholz *et al.* (1970)
2	Mastenbrook (1968) Balloon sounding, Trinidad	Constant concentration above 28 km
3	Estimated dry sky 0.002 gm kg^{-1}	Estimated dry sky 0.002 gm kg^{-1}
4	Sissenwine *et al.* (1968) Balloon sounding, Average observed profile	Scholz *et al.* (1970)

* Key profile.

other sources of opacity should be avoided as much as possible, but this would not usually be a problem at the band center. The region 630–685 cm^{-1} was chosen for the narrow (N) or opaque channel.

The second channel must receive enough energy from a more transparent portion of the spectrum for this part of the signal to have a high signal-to-noise ratio. Additional energy from the opaque region does not affect the results, so that a broad channel encompassing the two band wings around the central opaque region may be used. Two reasons exist for making this band as wide as possible; the first is to gain more energy, and the second is to see deeper into the atmosphere. As the band is made broader, other sources of atmospheric opacity begin to contaminate the signal and set limits on the band width.

The radiance was calculated as a function of frequency for 5-cm^{-1} intervals at several tangent heights, for each of the gases carbon dioxide ozone and water vapor. On the high-frequency side of the 15-μm band the signal due to the 14-μm O_3 band becomes large, in accordance with the results of Murcray *et al.* (1969), and water vapor gives an appreciable signal on the low side. Accordingly, the 585–705 cm^{-1} channel was chosen as the wide (W) channel. The effect of the 588-cm^{-1} N_2O band was not included. In the real atmosphere, the lower band limit would have to be somewhat higher.

8) FIELD OF VIEW SYNTHESIS

The spatial response function of the radiometer field of view (FOV) was assumed to be Gaussian, i.e.,

$$f(z-h) = (W\pi^{\frac{1}{2}})^{-1} \exp[-(z-h)^2/W^2]. \quad (18)$$

For a detector subtending an approximately 2-km altitude interval at the horizon, $W = 1.33$ km. Radiances were computed from 13–71 km in $\frac{1}{4}$-km increments, and the synthesized radiance

$$\bar{N}(h) = \int_{z=h-4}^{z=h+4} f(z-h)N(z)dz$$

calculated every kilometer. Here z is measured in kilometers.

9) NOISE

In addition to the finite field of view, a radiometer observation, even after calibration, will contain systematic and random noise. Systematic noise includes bias, n_B, a constant offset signal, and scale error in which the true signal is measured as a fixed multiple ϵ too high or too low. Random noise, $n_R(\sigma)$, is assumed to be Gaussian with standard deviation σ. A realistic radiance profile is then given by

$$N^*(h)=(1+\epsilon)\bar{N}(h)+n_B+n_R(\sigma).$$

The realistic data used below had $\epsilon=0.01$, $n_B=0.003$ W m^{-2} sr^{-1}, $\sigma=0.01$ W m^{-2}sr^{-1}. These values are well within the capabilities of an instrument with cooled detectors (J. R. Thomas, private communication).

c. The thickness between the 10- and 1-mb surfaces

The most useful quantity for dynamical calculations is generally not the temperature profile, but the thickness between two pressure surfaces, defined as

$$\Delta z=-\frac{R}{g}\int_{p_1}^{p_2}T(p)\frac{dp}{p}.$$

The vertical change in the geostrophic wind between two pressure surfaces may be calculated from the horizontal gradient of the thickness between the surfaces. Combining this change with geostrophic winds at the lower level gives the geostrophic winds at the upper level.

Winds are measured by balloons to levels up to 10 mb, and included in conventional map analyses. If the 10−1 mb thickness is known, knowledge of the geostrophic component of the wind will be extended to about 48 km. (Of course, this will not include tidal components or small-scale waves and turbulence.)

In the calculations described below, the heights of the 10 and 1 mb surfaces (among others) were obtained

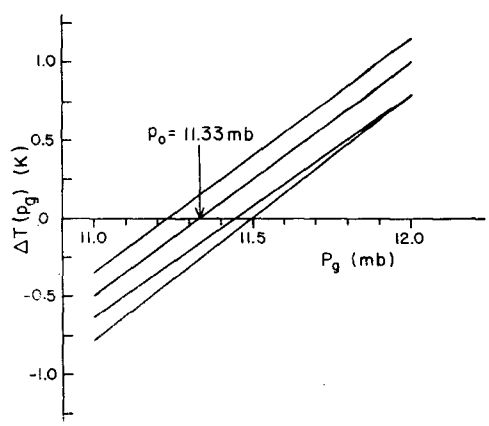

FIG. 8. Mean temperature difference $\Delta T(p_g)$ between the W and N channels over the 21–30 km height range vs p_g for inversions of realistic key atmosphere data. Each zero crossing gives an estimate $\hat{p}_0$ of the true pressure p_0.

TABLE 4. Inversion of realistic key atmosphere data at 1-km spacing.

Channel	Noise cases Narrow	Wide	$\hat{p}_0$ (mb)	rms temperature error (°K) 15–54 km	15–60 km	10–1 mb thickness error (m)
N*	1	1	11.45	2.99	3.71	22.0
	2	1	11.50	4.06	6.04	3.6
	1	2	11.23	3.39	4.10	48.1
	2	2	11.33	4.14	6.13	23.7
	average		11.38±0.12	3.65	5.00	24 ±18
W**	1	1	11.45	2.18	3.64	−14.1
	2	1	11.50	2.18	3.63	−20.1
	1	2	11.23	2.93	4.22	26.6
	2	2	11.33	2.87	4.14	14.3
	average		11.38±0.12	2.54	3.91	2 ±22

* 630–685 cm^{-1}
** 585–705 cm^{-1}.

by logarithmic interpolation between levels in the initial data and inverted results. The difference between the inverted and the actual thickness is the error of the thickness. As it is the gradient of the thickness in which we are interested, mean errors are not important, but the horizontal variability is crucial.

Of course, it would be possible to build winds up from a lower level (30 or 50 mb). That might be desirable if winds at those levels were sufficiently more accurate or more plentiful.

d. A detailed study of the key atmosphere with 1-km spacing

The crucial question is whether the $\hat{p}_0$ determination will work sufficiently well with real data to retrieve useful $\hat{p}_0$ values and allow accurate temperature determinations. To make as complete a test of the algorithm as possible, detailed studies were performed on the key atmosphere. Realistic data were synthesized for both the N and W channels, with two sets of random noise for each. Then each N-W pair of data sets were inverted with inversion levels spaced every kilometer in the vertical, for $p_g=11.00$ and 12.00 mb. The values of $\Delta T(p_g)$, averaged over the 21-30 km interval, are shown connected by straight lines in Fig. 8. Eq. (17) leads to the $\hat{p}_0$ values in Table 4. Taken together, they yield $\hat{p}_0=11.38\pm0.12$ mb, in excellent agreement with the correct 11.33 mb. (A similar study on this atmosphere, with data inverted every 3 km, gave $\hat{p}_0=11.28\pm0.10$ mb.)

Because both channels could be calibrated against the same blackbody in a real instrument, the systematic (scale and bias) errors should be similar in the two channels. In that event, these errors have negligible effect on the $\hat{p}_0$ determination.

These values of $\hat{p}_0$ were then used for inversions of the appropriate radiance data. Wide (W) channel inversions for the true noise distributions are compared to the initial profile in Fig. 9. Note that this is the same atmosphere that was inverted with errorless data in Fig. 4. The general conclusion one gets from Fig. 9 is that the larger features are still reproduced quite well to above 50 km. Above that level, large oscillations

are seen. Small features, notably the thin warm region at 37 km, are now completely missed. An inspection of Table 4, which summarizes all the results of this test, leads to the following conclusions:

1) All error sources contribute approximately ±0.12 mb to the p_0 estimation. For the noise distributions used, $\hat{p}_0$ is more sensitive to the W channel noise, but this is probably not a general result.

2) The broad channel results are distinctly better for temperature determination.

3) If one takes a 3K rms temperature error as a criterion for data to be meteorologically useful, results inverted in the W channel are satisfactory from 15–54 km.

4) The errors are larger in the upper part of the solution, especially in the 54–60 km region.

The latter effect is due to the reduced signal-to-noise ratio as the radiance drops to small values at high altitudes. As we shall see below, wider spacing of inverted levels can improve the high level retrieval.

e. Sensitivity of results to the vertical spacing of inverted points, field of view and noise

For a known p_0, the accuracy of the inversion will depend not only on the FOV and the noise, but also on the vertical spacing of the inversion levels, which is arbitrary. The finite width of the weighting functions suggests that inversion at levels very close together will not yield significantly more information than at levels further apart. At the other extreme, inversion levels spaced too far apart will miss significant structure that could be resolved. We assume the radiance measurements are spaced 1 km in the vertical. It does not appear to be fruitful to determine more temperatures than measurements, as Smith (1970) does.

To investigate sensitivity to these factors, a hierarchy of cases was run based on the key profile, which had considerable fine structure. In the first case, there was no noise in the data, infinite vertical resolution (instrument response given by the delta "function"), and inversion levels spaced every kilometer. As the correct p_0 was used, this corresponds to an ideal case, or the limit of the algorithm. It is important to note that although there was no noise in the data, the temperature profile was iterated only until the rms difference between the calculated and "measured" radiance was less than 0.01 W m^{-2} sr^{-1}, the value used for realistic data with noise. Had the convergence criterion been reduced, the difference between the initial and inverted temperature profiles could have been made arbitrarily small.

The result for this first case was compared to the initial profile in Fig. 4. The rms difference between the initial and inverted temperature profiles is 0.9K for the W channel, from 15–54 km. This is likely to be too optimistic, since the points on the initial profile at

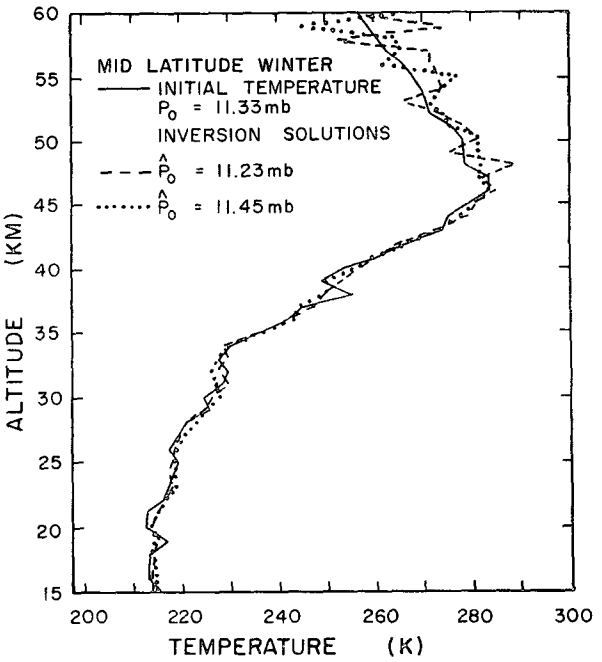

FIG. 9. Temperature solutions obtained by blind inversions of realistic (noisy) data. In each case N and W channel data were used to determine $\hat{p}_0$, which was then used with the wide channel data to obtain the temperature distribution.

which changes of slope occurred were all on even kilometer levels, where the inverted values were obtained. Fig. 4 also shows the inversion of data having the 2-km FOV described above, but free of noise. With infinite resolution, the small changes of profile above about 22 km are followed very closely. The 2-km FOV follows the larger features, but cannot readily follow the smallest ones. The rms temperature error is 1.6K for this profile.

The results of a number of such studies are shown in Fig. 10, in which the rms temperature error from 15–54 km is plotted against the spacing of the inverted levels. For noise-free data with infinite vertical resolution (open circles) we see that the error increases sharply as the level spacing increases from 1 to 3 km, indicating that we are losing information. For noise-free data with a 2-km FOV (x's), which therefore smear some of the fine structure, there is a larger error at 1-km spacing, as discussed above, but a much smaller loss of accuracy as the spacing of inversion points is increased. At 3-km spacing, the finite FOV signal actually yields a lower rms error because it contains some information from the regions adjacent to the inversion level which the infinite resolution signal does not have. At 1-km spacing, the addition of the 2-km FOV increases the error variance by 1.70 deg^2.

The addition of 0.01 W m^{-2} sr^{-1} random noise to data with infinite vertical resolution (closed circles) adds 4.23 deg^2 to the variance, demonstrating that it

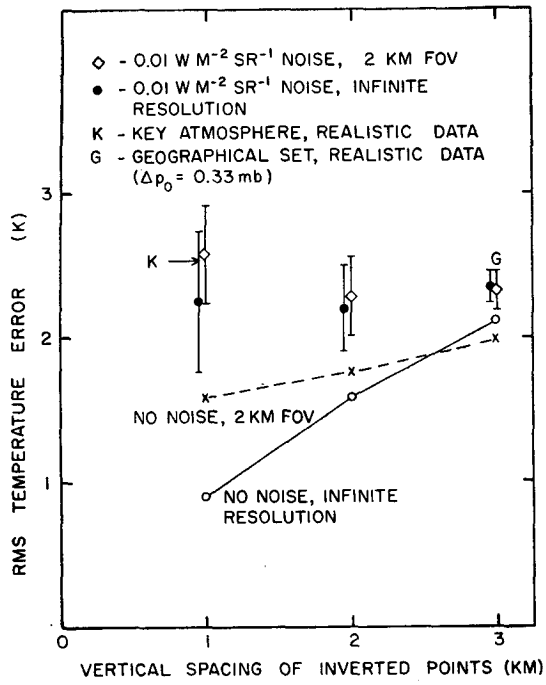

FIG. 10. Dependence of rms temperature error of the inversion from 15–54 km as a function of level spacing, field of view and 0.01 W m^{-2} sr^{-1} random noise. For comparison, results of the blind key atmosphere inversions (Table 4) and the inversions of the geographical set (Table 5) are also shown.

is principally responsible for the degradation of accuracy. The error bars indicate the standard deviation of the inferred temperature errors. With this noisy data, there is no loss of accuracy as the level spacing increases. The same is also true for noisy data having 2-km FOV (diamonds). At 1-km spacing the error is somewhat larger than at 2- or 3-km spacing.

For comparison, the mean of the results of the key profile inversions discussed in Section 5d and summarized in Table 4 is shown by the K in Fig. 10. Those data included, in addition to random noise and FOV, the effects of systematic instrument error, pressure errors and signal contamination by ozone and water vapor. The numbers and Fig. 10 indicate that the temperature errors agree, and suggest that the other errors make a rather small additional contribution to the effects of FOV and noise. They also imply with this noise level that there are no more than $(54-15)/3=13$ independent determinable pieces of information between 15 and 54 km.

We conclude that we can perform many exploratory studies with 3-km spacing of inverted points, at a considerable saving in computer time, knowing that the results will be similar to those obtained with more closely spaced levels. Results of inverting realistic data at 3-km spacing for the range of geographical situations to be discussed in Section 5f are indicated in Fig. 10 by G. The agreement supports the conclusions on the size of the temperature error, and the dominant contributions of noise and FOV.

f. Sensitivity of inversion solutions to geographical and seasonal variations

In order to establish the usefulness of the technique described here, it must be shown to work comparably well for the large variety of geographical and seasonal situations which might be encountered. Rather than performing the same kind of detailed studies described above for a large number of atmospheres, an alternate method which is more illuminating as well as requiring less computer time was employed to obtain the information.

Because errors in $\hat{p}_0$ lead to systematic temperature errors, and thus errors in thickness, the $\hat{p}_0$ determination was identified as a crucial element. The geographical variability of $\hat{p}_0$ was studied by inverting error-free data for the six temperature profiles described in Section 5b and Table 1. An auxiliary investigation showed that $\hat{p}_0$ was virtually unchanged if the H_2O and O_3 were neglected in both synthesis and inversion, and if inversion levels were spaced 3 km apart. The results are shown in Fig. 11. The pressure scale is now relative to p_0, which is different for each profile. The results taken together give $\hat{p}_0=p_0-0.17\pm0.28$ mb.

The figure also shows that much of the variability is due to profile 5, the tropical sounding with a cold tropopause. Without this, one gets $\hat{p}_0=p_0-0.08\pm0.21$ mb, which applies to extratropical regions. It is likely that improvements will make the accuracy comparable in tropical regions. Another study (not shown), in which the variations in O_3 and H_2O were included in the synthesis, but not in the inversion, gave for the extratropical atmospheres $\hat{p}_0=p_0+0.49\pm0.12$ mb. Thus, the geographical spread is likely to be between 0.12 and

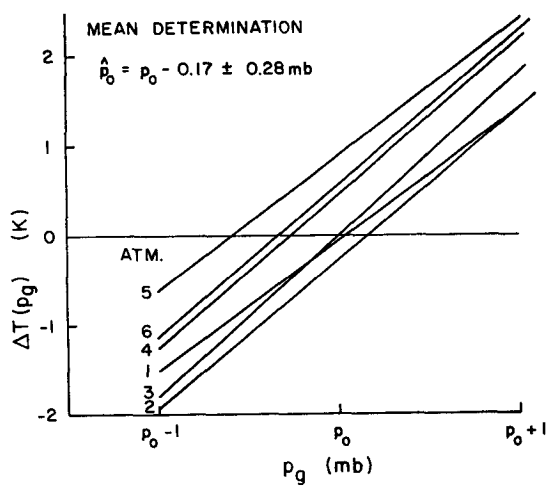

FIG. 11. Mean 21–30 km temperature differences between N and W channels for six different temperature profiles (atmospheres). This indicates geographical and seasonal variability of the $\hat{p}_0$ determination.

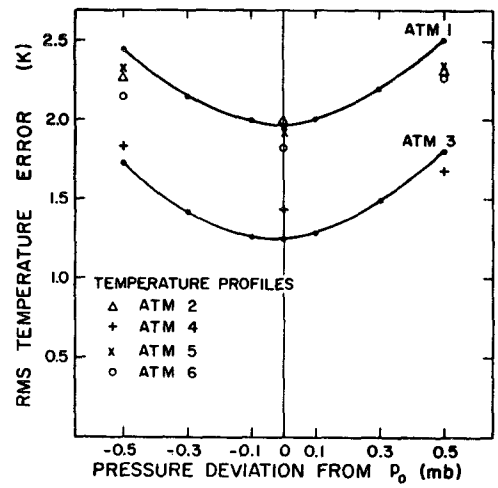

FIG. 12. Dependence of rms temperature error on p_0 error for six temperature profiles.

0.28 mb. (The spread is more important than the offset, because the latter can be corrected, and also because it is the horizontal *variation* of thickness errors which will limit the ability to derive thermal winds, not the errors themselves.)

Combining the variations due to instrument noise (0.12 mb) with that due to geographic variability (0.12 or 0.28 mb), we find a total variability in p_0 between 0.17 and 0.30 mb. The nature of the dependence of the rms temperature error on $\hat{p}_0$ is illustrated in Fig. 12. The points result from inverting error-free data with infinite resolution at 3-km spacing for the six climatological temperature profiles. They indicate that the dependence is relatively slight. Combining these values with the noise contribution to temperature error variance (1.12 deg^2 from Fig. 10) leads to the conclusion that any $\hat{p}_0$ within 0.5 mb of p_0 will give useful results.

The 10- to 1-mb thickness errors are expected to be more sensitive to p_0 estimation, since errors in $\hat{p}_0$ lead to systematic errors in temperature. Using 3-km inversions, this error is plotted as a function of p_0 errors in Fig. 13, for the six temperature profiles. We note, even with the correct pressure, that we have $\Delta z = -23 \pm 10$ m. (Because thicknesses are differentiated in the horizontal to get thermal winds, the constant error does not matter, but the variability does.) The mean slope is approximately -150 m mb^{-1}.

Inverting four sets of noisy data for the key temperature profile with the correct p_0, the result obtained was $\Delta z = -37 \pm 11$ m. We may now calculate expected thickness errors from

$$\sigma_{\Delta z}^2 = \left(\frac{\partial(\Delta z)}{\partial p_0}\right)^2 \sigma_{\hat{p}_0}^2 + (\sigma_{\Delta z})_{p_0}^2 + (\sigma_{\Delta z})^2_{\text{NOISE}}$$

$$= (150)^2 \sigma_{\hat{p}_0}^2 + 10^2 + 11^2, \quad (19)$$

from which $\sigma_{\Delta z}$ is 30 m with $\sigma_{\hat{p}_0} = 0.17$ mb and 52 m with $\sigma_{\hat{p}_0} = 0.33$ mb. As expected, the dependence on $\hat{p}_0$ is the dominant effect.

For comparison, in mid-latitudes, with soundings spaced 1000 km apart, an error of ± 70 m leads to a 10 m sec^{-1} error in the thermal wind, or about 10% of the maximum winds observed at these levels (Staff, NMC, 1969). If this is taken as the accuracy required for useful measurements, the $\hat{p}_0$ error must be less than ± 0.46 mb.

To verify these predictions, realistic W channel data, which included the effects of particular O_3 and H_2O distributions were calculated. Errors of about ± 0.17 and ± 0.33 mb were added to the correct p_0, and inversions were performed, assuming an average O_3 or H_2O distribution.

Some results are shown in Figs. 14–16. Fig. 14 shows the key atmosphere, seen previously, inverted at 3-km intervals. The 2-km wide feature at 37 km is not seen, but agreement through most of the profile is quite good. The oscillations at the top of the inversion are considerably reduced. The wider spacing at the upper levels improves the stability at the solution, and improves the rms temperature accuracy. The inversion for the tropical atmosphere in Fig. 15 shows the present difficulty in retrieving the very cold tropical tropopause at 18 km. The broad variation around 36 km in Fig. 16 is reproduced reasonably well, for both pressure errors, while the narrow, weaker feature near 25 km is not. We also note in Figs. 14–16 that below about 45 km there is rather little difference between the $\Delta p_0 = 0.17$ and 0.33 mb curves. Above that level the 0.33 mb curve is not as accurate on the average.

Study of plots of individual solutions suggests that ozone and water vapor variations do not appreciably

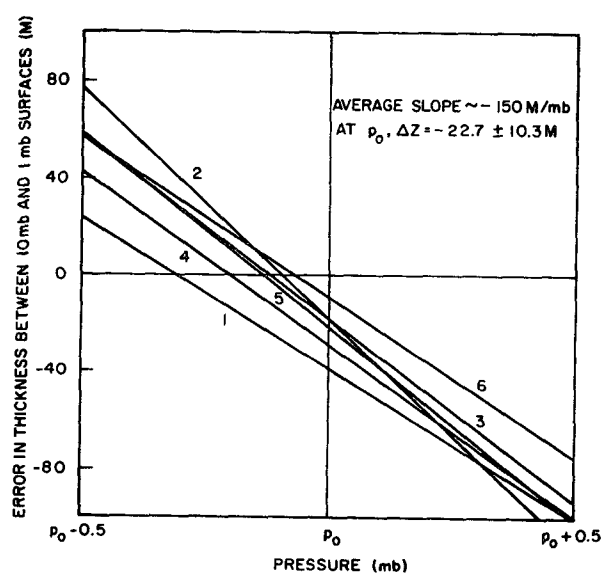

FIG. 13. Dependence of 10- to 1-mb thickness errors on p_0 error for six temperature profiles.

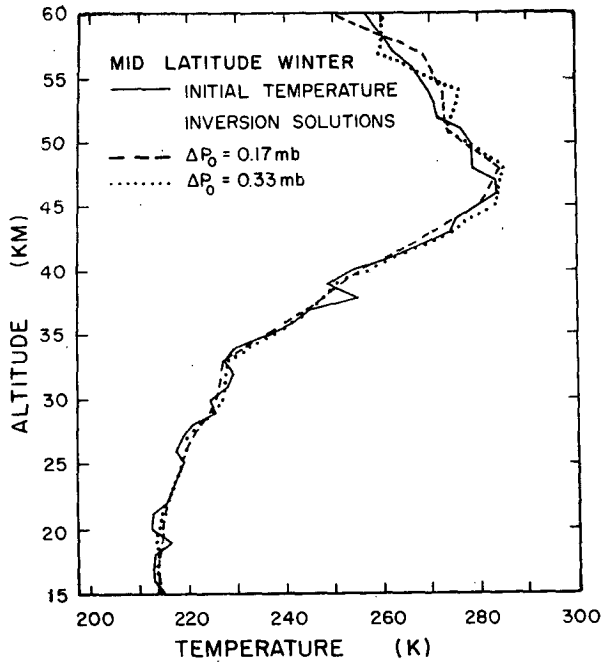

FIG. 14. Mid-latitude winter sounding (key atmosphere), with inverted points every 3 km, for $\Delta p_0=0.17$ and 0.33 mb.

alter the inferred temperature distribution. It does not appear necessary to iterate between a temperature and a constituent inversion.

The results of all cases are summarized in Table 5. We note that with the 3-km vertical resolution, ΔT_{rms} <3K up to 60 km for either pressure error. This

TABLE 5. Results of temperature inversions for a range of geographical and seasonal conditions. Inverted levels are spaced 3 km apart.

Profile combination (atmosphere numbers)			$\Delta p_0=0.17$ mb		$\Delta p_0=0.33$ mb	
T	O_3	H_2O	ΔT_{rms} 15–54 km (°K)	Thickness error (m)	ΔT_{rms} 15–54 km (°K)	Thickness error (m)
1	1	1	2.34	−46	2.65	11
1	2	1	2.13	0	2.43	59
1	4	1	2.61	29	2.33	17
1	4	4	2.52	49	2.48	7
2	1	1	2.09	−62	3.29	47
3	1	3	1.87	15	2.32	−72
5	2	2	2.24	17	2.67	93
6	4	4	2.24	68	2.05	5
rms			2.26	9±44	2.53	21±49
Desirable			3.	±70	3.	±70

corroborates the general conclusion reached above, and indicates that better inferences may be obtained at the higher levels with greater spacing. It also illustrates the smoothing property of the algorithm.

The variability of the thickness error is about the same as suggested by the error propagation analysis, although the dependence on $\hat{p}_0$ error is not as great. The agreement supports our assumptions and the conclusions about the size of the errors that may be expected.

6. Conclusions

We have presented a theoretical analysis to demonstrate that the limb radiance profile depends upon the

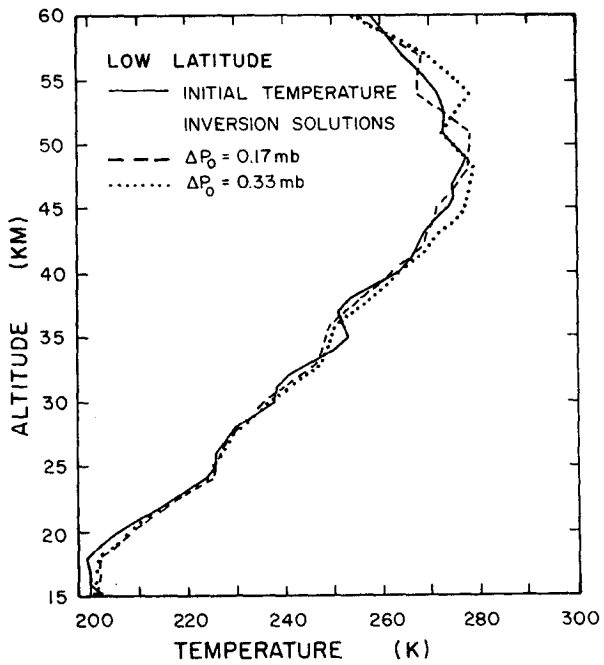

FIG. 15. Tropical sounding with inverted points every 3 km, for $\Delta p_0=0.17$ and 0.33 mb.

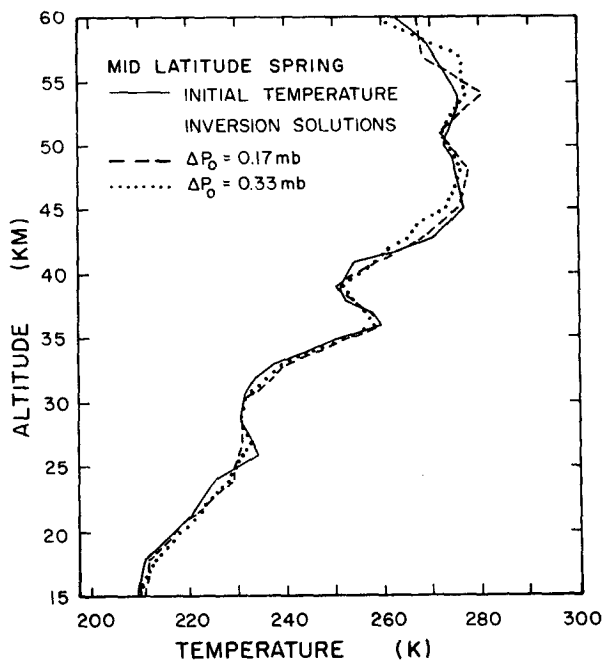

FIG. 16. Mid-latitude spring sounding with inverted points every 3 km, for $\Delta p_0=0.17$ and 0.33 mb.

pressure p_0 at one elevation and the temperature distribution. From this, it follows that if p_0 is known at one elevation z_0 it should be possible to invert a measured limb radiance profile to yield a temperature distribution as a function of altitude *relative* to z_0. The results presented in Fig. 4 showed that this is indeed possible for error-free data.

The fact that errors in p_0 lead to systematic temperature errors leads to a method of estimating p_0 from measurements in two channels, and the definition of the estimate, $\hat{p}_0$, as that pressure which minimizes the mean difference between temperatures inferred from the two channels.

The inversion of data for real atmospheres, containing the effects of a 2-km field of view, radiation from trace gases, and instrumental noise, demonstrates that the method yields very good results in realistic situations. In particular, the error in $\hat{p}_0$ with the present algorithm is about 0.30 mb when p_0 is about 11 mb. It is anticipated that improvements will reduce this to the 0.17 mb now obtained in extratropical latitudes. With either figure, the rms temperature error is $\leqslant 2.6$K from 15–54 km, and less than 3K from 15–60 km. The error in thickness from 10–1 mb is $\leqslant 49$ m, which corresponds to a 7 m sec^{-1} uncertainty in the thermal wind over this layer for mid-latitude measurements spaced 1000 km apart.

As in other inversion schemes, the principal limitation to the accuracy is the random noise in the measurements. The figures used here are rather conservative; it seems likely that an instrument could be built having random noise only one-fifth of the value used here. That suggests that the upper limiting altitude will be roughly (scale height)$\times \ln 5 \approx 12$ km higher. Averaging vertically and between the W and N channel results should further reduce the noise and allow temperatures to be obtained to perhaps 75 km. This region of the atmosphere, between the stratopause and the mesopause, is rarely sounded at the present time.

In this region of the atmosphere we must consider the possibility of departures from local thermodynamic equilibrium (Kuhn and London, 1969; Drayson, 1967). In that instance, measurements might be most usefully interpreted as *in situ* determinations of collisional relaxation times.

The inversion of limb radiance measurements appears to hold considerable potential as a method for exploring the atmosphere above the tropopause, and possibly almost to the mesopause.

Acknowledgments. We thank Mr. John R. Thomas of Honeywell, Inc., for many stimulating conversations and Mr. Paul Bailey for assistance with the last set of calculations. This research was primarily supported by NASA Contract NAS5-21177, by the Atmospheric Sciences Section, National Science Foundation, under Grants GA 10838 and 20213, and by computer time from the National Center for Atmospheric Research, Boulder, Colo., and the Florida State University computing center. JCG acknowledges the hospitality of the Department of Astro-geophysics, University of Colorado, especially Prof. Julius London, and of the National Center for Atmospheric Research during visits at those institutions.

REFERENCES

Bandeen, W. R., B. J. Conrath and R. A. Hanel, 1963: Experimental confirmation from the Tiros VII meteorological satellite of the theoretically calculated radiance of the earth within the 15-micron band of carbon dioxide. *J. Atmos. Sci.*, **20**, 609–614.

Bates, J. C., 1967: Spectral analysis of the spatial distribution of the earth's 15 μ carbon dioxide horizon profile. *Infrared Phys.*, **7**, 181–194.

——, D. S. Hanson, F. B. House, R. O'B. Carpenter and J. C. Gille, 1967: The synthesis at 15 μ infrared horizon radiance profiles from meteorological data inputs. NASA CR-724, 294 pp.

Burn, J. W., and W. G. Uplinger, 1970: The determination of atmospheric temperature profiles from planetary limb radiance profiles. NASA CR 1513, 83 pp.

Chahine, M. T., 1968: Determination of the temperature profile in an atmosphere from its outgoing radiation. *J. Opt. Soc. Amer.*, **58**, 1634–1637.

——, 1970: Inverse problems in radiative transfer: Determination of atmospheric parameters. *J. Atmos. Sci.*, **27**, 960–967.

Drayson, R., 1967: Calculation of long wave radiative transfer in planetary atmospheres. Rept. 07584-1-T., University of Michigan, Ann Arbor College of Engineering.

Gille, J. C., 1968: On the possibility of estimating diurnal temperature variations of the stratopause from horizon radiance measurements. *J. Geophys. Res.*, **73**, 1863–1868.

Girard, A., and M. P. Lemaitre, 1970: Profils experimentaux de l'horizon infrarouge de la terre. *Appl. Opt.*, **9**, 903–912.

Goody, R. M., 1964: *Atmospheric Radiation. I. Theoretical basis.* London, Oxford University Press, 424 pp.

Hanel, R., W. Bandeen and B. Conrath, 1963: The infrared horizon of the planet earth. *J. Atmos. Sci.*, **20**, 73–86.

Hilsenrath, E., 1971: Ozone measurements in the mesosphere and stratosphere during two significant geophysical events. *J. Atmos. Sci.*, **28**, 295–297.

——, L. Seiden and P. Goodman, 1969: An ozone measurement in the mesosphere and stratosphere by means of a rocket sonde. *J. Geophys. Res.*, **64**, 6873–6880.

Houghton, J. T., and S. D. Smith, 1970: Remote sounding of atmospheric temperature from satellites I. Introduction. *Proc. Roy. Soc. London*, **A320**, 23–33.

House, F. B., and G. Ohring, 1969: Inference of stratospheric temperature and moisture variables from observation of the infrared horizon. NASA CR-1419, 58 pp.

Hunt, B. G., 1966a: The need for a modified photochemical theory of the ozonosphere. *J. Atmos. Sci.*, **24**, 88–95.

——, 1966b: Photochemistry of ozone in a moist atmosphere. *J. Geophys. Res.*, **71**, 1385–1398.

Komhyr, W. D., and P. R. Sticksel, 1967: Ozonesonde observations, 1962–1966. ESSA Tech. Rept. 1ER51-LAS7.

Kondrat'yev, K. Ya, and K. E. Yakushevskaya, 1963: The distribution of outgoing thermal radiation in the different regions of the spectrum. *Proceedings International Symposium on Rocket Satellite Meteorology*, Amsterdam, North Holland Publ. Co., p. 254.

Kuhn, W. R., and J. London, 1969: Infrared radiative cooling in the middle atmosphere (30–110 km). *J. Atmos. Sci.*, **26**, 189–204.

Mastenbrook, H. J., 1968: Water vapor distributions of the stratosphere and high troposphere. *J. Atmos. Sci.*, **25**, 299–311.

McKee, T. B., 1970: Inference of temperature and water vapor structure in the stratosphere from limb radiance profiles. NASA TM X-1943, 23 pp.

——, R. I. Whitman and R. E. Davis, 1968: Infrared horizon profile for summer conditions from project scanner. NASA TN-D-4741, 121 pp.

——, ——, and J. J. Lambiotte, Jr., 1969: A technique to infer atmospheric temperature from horizon radiance profiles. NASA TN D-5068, 31 pp. (CFSTI).

Murcray, D. G., F. H. Murcray, W. J. Williams, T. G. Kyle and A. Goldman, 1969: Variation of the infrared solar spectrum between 700 cm^{-1} and 2240 cm^{-1} with altitude. *Appl. Opt.*, **8**, 2519–2536.

Rodgers, C. D., and C. D. Walshaw, 1966: The computation of infrared cooling rates in planetary atmospheres. *Quart. J. Roy. Meteor. Soc.*, **92**, 67–92.

Scholz, T. C., D. H. Ehhalt, L. E. Heidt and E. A. Martell, 1970: Water vapor, molecular hydrogen, methane and tritium concentrations near the stratopause. *J. Geophys. Res.*, **75**, 3049–3054.

Sissenwine, N., D. D. Grantham and H. A. Salmela, 1968: Mid-latitude humidity to 32 km. *J. Atmos. Sci.*, **25**, 1129–1140.

Smith, W. L., 1969a: Statistical estimation of the atmosphere's geopotential height distribution from satellite radiation measurements. ESSA Tech. Rept. NESC 48.

——, 1969b: A polynomial representation of carbon dioxide and water vapor transmission. ESSA Tech. Rept. NESC 47.

——, 1970: Iterative solution of the radiative transfer equation for the temperature and absorbing gas profile of an atmosphere. *Appl. Opt.*, **9**, 1993–1999.

Staff, NMC, 1969: Weekly synoptic analyses, 5-, 2- and 0.4-millibar surfaces for 1966. ESSA Tech. Rept. WB-9.

Walker, R. G., C. V. Cunniff and A. P. D'Agati, 1966: Measurement of the infrared horizon of the earth. Air Force Cambridge Research Laboratories, Environmental Research Papers No. 223, AFCRL-66-631.

Wark, D. Q., 1970: SIRS: An experiment to measure the free air temperature from a satellite. *Appl. Opt.*, **9**, 1761–1766.

——, J. Alishouse and G. Yamamoto, 1964: Variation of the infrared spectral radiance near the limb of the earth. *Appl. Opt.*, **3**, 221–227.

Whitman, R. I., T. B. McKee and R. E. Davis, 1968: Infrared horizon profiles for winter conditions from project scanner. NASA TN D-4950. 125 pp.